Assessing methods for geometric distortion compensation in 7T gradient echo fMRI data

Michael-Paul Schallmo[1*], Kimberly B. Weldon[2,1], Scott R. Sponheim[3,1], & Cheryl A. Olman[4,2]

[1]Department of Psychiatry and Behavioral Sciences, University of Minnesota, Minneapolis, MN
[2]Center for Magnetic Resonance Research, University of Minnesota, Minneapolis, MN
[3]Veterans Affairs Medical Center, Minneapolis, MN
[4]Department of Psychology, University of Minnesota, Minneapolis, MN

[*]corresponding author: schal110@umn.edu

Abstract

Echo planar imaging (EPI) is widely used in functional and diffusion-weighted MRI, but suffers from significant geometric distortions in the phase encoding direction caused by inhomogeneities in the static magnetic field (B_0). This is a particular challenge for EPI at very high field (7T and above), as distortion increases with higher field strength. A number of techniques for correcting geometric distortion exist, including those based on B_0 field mapping and acquiring EPI scans with opposite phase encoding directions. However, few quantitative comparisons of distortion compensation methods have been performed using EPI data from the human brain, and even fewer at very high field. In the current study, we compared geometric distortion compensation using B_0 field maps and opposite phase encoding scans implemented in two different software packages (FSL and AFNI) applied to 7T gradient echo EPI data from 31 human participants. We assessed the quality of distortion compensation by quantifying the degree of alignment to a T_1-weighted anatomical reference scan using Dice coefficients and mutual information. We found that the best distortion compensation was achieved in our dataset using gradient echo scans with opposite phase encoding directions to map the distortion, as compared to B_0 field maps or spin echo opposite phase encoding scans. Performance between FSL and AFNI was equivalent. While the ideal geometric distortion compensation approach may vary due to methodological differences across experiments, this study provides a framework for researchers to assess the quality of different distortion compensation methods in their own work.

Introduction

Geometric fidelity is critical for high quality brain imaging. It is essential for accurate interpretation of functional MRI (fMRI) data based on anatomical landmarks and is necessary for precise quantification of structural and functional connectivity. It is also relevant for clinical brain imaging applications, such as neurosurgery and the placement of deep brain stimulation electrodes. However, currently-popular MRI techniques suffer from a number of common artifacts that degrade spatial fidelity, including gradient nonlinearities and geometric distortion due to B_0 inhomogeneity[2, 3]. A number of methods to correct for these geometric artifacts have been established[2-5]. To select an appropriate method for distortion correction, quantitative comparisons between methods are essential, but few of these studies have been performed to-date.

Echo planar imaging (EPI) is among the most commonly used MRI techniques in human neuroscience. Rapid acquisition times enable studies of functional brain activation (i.e., fMRI; often ≤ 1 s per whole-brain image) and efficient measurement of white matter tractography via diffusion-weighted MRI (dMRI; on the order of 5 s per image). This temporal efficiency comes at the cost of relatively low pixel bandwidth in the phase encoding (PE) direction, which results in severe geometric distortions in regions of B_0 inhomogeneity[3-5]. Lower bandwidth (i.e., higher effective echo spacing) makes distortion more severe; distortion of some regions in EPI data in the PE direction often reaches 5-10 mm[3]. B_0 inhomogeneities and the resulting distortions are greatest at the interface of different tissue types (e.g., brain, bone, air) in regions such as the orbitofrontal cortex and temporal lobes. Inhomogeneities also scale linearly with B_0 field strength,

such that geometric distortions are more severe at 7 Tesla than at 3 Tesla[6] (though this is mitigated by the fact that smaller voxel sizes typically achieved at higher field will reduce distortion).

A number of methods for minimizing and correcting geometric distortion in EPI data exist. Prospectively, geometric distortion can be limited by reducing B_0 inhomogeneity via B_0 shimming and confirming shim quality during a scan by measuring the linewidth of the water signal. Geometric distortion can also be limited by shortening read-out time. Methods for this include: 1) using multi-shot or segmented EPI[7-9] (rather than single-shot sequences, at the cost of longer TRs and increased physiological noise sensitivity), 2) using a higher parallel imaging acceleration factor (R; assuming the radio frequency coil has multiple receive elements, at the cost of reduced signal-to-noise ratio [SNR]), 3) increasing receiver bandwidth (i.e., reducing echo spacing, at the cost of reduced SNR), 4) decreasing the field of view in the PE direction (at the cost of reduced spatial coverage)[10]. Although one might be tempted to think that distortion would also be attenuated by reducing the sampling of *k*-space data in the PE direction using partial Fourier approaches, this is not the case; distortion is just as bad for partial Fourier data as it would be with full sampling because phase errors in the sampled portion of *k*-space are extrapolated. Finally, it is worth noting that when using spiral acquisition sequences[11] in place of EPI, B_0 inhomogeneity produces blurring rather than geometric distortion, which may be preferable for some applications.

It is also possible to correct geometric distortion in an EPI dataset retrospectively, which has been shown to improve registration between EPI and T_1-weighted anatomical data[4]. A number of different methods for retrospective distortion compensation have been introduced, including:

1) B_0 field mapping by measuring phase differences from two gradient echo (GE) images with different echo times (TEs)[4, 12, 13],
2) calculating a distortion field based on two EPI scans with opposite PE directions (i.e. forward & reverse, often anterior-posterior and posterior-anterior; hereafter referred to as opposite phase encoding [oppPE] field mapping), for which the geometric distortion will be equal but in opposite directions[14-16],
3) non-rigid registration (e.g., affine or spline fitting) of the distorted EPI to a minimally distorted anatomical reference[17-21],
4) mapping the EPI point-spread function[22-24],
5) methods based on forward and inverse modeling of the distortion[25, 26],
6) multi-reference scan methods[27],
7) hybrid methods (e.g., B_0 or oppPE field mapping plus non-rigid registration)[5, 13, 28], and
8) dynamic methods for correcting time-varying geometric distortions due to factors such as head movement[6, 26, 29].

Of these, the first two (B_0 and oppPE field maps) are arguably the most popular and are currently implemented in various forms across many widely used MRI analysis software packages (e.g., FSL[30], AFNI[31], SPM[32], BrainVoyager[33]). Thus, we chose to focus on quantitative comparisons between B_0 and oppPE field map approaches in the current study.

With regard to oppPE field maps, it has been suggested that spin echo (SE) EPI scans may offer an advantage over GE sequences in mapping the distortion field[34], as the former minimizes signal dropout from through-slice dephasing due to the 180° refocusing pulse at TE/2. This suggests that a pair of SE EPI scans with opposite PE directions should give a more complete map of field inhomogeneities than a GE oppPE pair. However, this theoretical motivation has not, to our knowledge, been tested empirically, and other factors (e.g., increased subject motion due to added scan time, image intensity differences) might limit the utility of SE oppPE field maps for the correction of geometric distortion in GE EPI data, which is currently the most commonly used technique for fMRI. Thus, in the current study we sought to directly and quantitatively compare the performance of SE and GE oppPE field maps applied to GE EPI data.

Previous studies that have compared different methods for geometric distortion compensation have generally focused on data collected at field strengths of 1.5 to 3T, for which geometric distortion may be less extreme as compared to very high field (≥ 7T). The proliferation of very high field imaging methods[35], due in part to efforts such as the Human Connectome Project[36-40], makes it increasingly important to achieve effective geometric distortion compensation of high field EPI data. Therefore, in the current study we examined this issue using 7T EPI data that we have collected as part of the Psychosis Human Connectome Project at the University of Minnesota's Center for Magnetic Resonance Research.

Prior investigations of geometric distortion compensation methods have not, generally, included correction for additional gradient nonlinearities[41]. Gradient nonlinearities are unrelated to distortion due to B_0 inhomogeneity, are present in all three dimensions (PE, readout, and through-slice), and are sequence independent[2]. These gradient

nonlinearities can be on the order of 1-2%[2, 3] and will vary between scanners due to differences in gradient hardware. Distortions due to gradient nonlinearities may therefore confound efforts to achieve high spatial fidelity in EPI data, and are particularly important to consider when trying to unify datasets acquired on different scanners (e.g., a T_1 anatomy acquired at 3T, and GE EPI fMRI data acquired at 7T, as in the current study).

In this study, we compared the methods noted above (i.e., GE and SE oppPE as well as B_0 field maps) for the correction of geometric distortion due to B_0 inhomogeneity in GE EPI data collected at very high field (7T), following a separate correction for gradient nonlinearity distortion. We sought to answer the following question: which distortion compensation method(s) would perform best for our 7T GE fMRI data? This study presents a framework within which to answer this question for a given data set. We do not intend to prescribe one method as definitively superior over another in all cases, as relative performance is expected to depend on acquisition parameters, order and timing of the acquisition of EPI and field map scans, scanner and radiofrequency coil hardware, and the details of the processing pipeline that is used. Our results suggest that all of the examined methods improved correspondence between GE EPI and T_1 anatomical data, with the best performance being observed for GE oppPE field map methods in our dataset.

Methods

Participants

We recruited 31 participants for the current study from a larger sample as part of the Psychosis Human Connectome Project. This included 12 patients with a diagnosed psychotic disorder (e.g., schizophrenia), 9 first-degree biological relatives of patients with psychosis (i.e., parents, siblings, or children), and 10 healthy controls. Group differences were not examined in this particular study, as a subject's mental health status was not deemed relevant to the assessment of geometric distortion compensation methods. We chose to study a diverse population (i.e., patients and controls) in order to make our results more broadly applicable to the type of MRI data that would be obtained in clinical populations such as adults with psychosis. Subject demographics were as follows: 20 female and 11 male participants, mean age was 45 years (*SD* = 11 years).

Inclusion criteria for the Psychosis Human Connectome Project were as follows: age 18-65 years, English as primary language, the ability to provide informed consent, no legal guardian, no alcohol or drug abuse within the last 2 weeks, no alcohol or drug dependence within the last 6 months, no diagnosed learning disability or IQ less than 70, no current or past central nervous system disease, no history of head injury with skull fracture or loss of consciousness longer than 30 min, no electroconvulsive therapy within the last year, no tardive dyskinesia, no visual or hearing impairment, no condition that would inhibit task performance such as paralysis or severe arthritis. All patients had a history of bipolar I, schizophrenia, or schizoaffective disorder and were not adopted. Relatives had a biological parent, sibling, or child with a history of one of these disorders and were not adopted. Controls had no personal or family history (parents, siblings, children) of these disorders. Additional inclusion criteria for this particular study included the ability to fit comfortably within the scanner bore (60 cm diameter) and the radio frequency head coil (head circumference less than 62 cm), weight less than 440 pounds, and corrected Snellen visual acuity of 20/40 or better. Further, all participants had completed two 3T fMRI scanning sessions prior to 7T scanning and did not exceed a limit of 0.5 mm of head motion across greater than 20% of TRs from all 3T fMRI runs (approximately 2 hours of scanning). Finally, participants included in this study had all 7T MRI scans acquired in the prescribed order (see below) and did not exceed a limit of 0.5 mm of head motion on greater than 20% of TRs during 7T fMRI scans (1.25 hours of scanning).

All participants provided written informed consent prior to participation and were compensated for their time. All experimental procedures complied with the regulations for research on human subjects described in the Declaration of Helsinki and were approved by the Institutional Review Board at the University of Minnesota. All subjects were found to have sufficient capacity to provide informed consent, as assessed by the University of California Brief Assessment of Capacity to Consent[42].

Experimental protocol

7T MRI data were acquired on a Siemens MAGNETOM scanner (software version: VB17). This scanner was equipped with an 8-kW radio frequency power amplifier and body gradients with 70 mT/m maximum amplitude and 200 T/m/s maximum slew rate. We used a Nova Medical (Wilmington, MA) radio frequency head coil with 1 transmit and 32 receive channels for all 7T MRI data acquisition. Subjects were provided with head padding inside the coil and instructed to

minimize head movements during scanning. We placed 5 mm thick dielectric pads (3:1 calcium titanate powder in water) under the neck and beside the temples, as this has been shown to improve transmit B_1 homogeneity in the cerebellum and temporal lobe regions during 7T MRI[37].

MRI data were acquired using sequences and scan parameters that followed the original young adult Human Connectome Project[36-40]. Parameters for the different MR scans are listed in Table 1. Additional scan parameters include a multiband acceleration factor of 5 for GE and SE fMRI, and GRAPPA parallel imaging acceleration factor (R) of 2 for all scans except the B_0 field map (no acceleration). The delta TE for the B_0 field map scan was 1.02 ms. Single-band reference scans were acquired with each multi-band EPI scan (GE & SE). Data were acquired using Siemens Auto Align to standardize the orientation and positioning of the imaging field of view.

7T MRI data in this study were acquired in a fixed scan order:

1) auto-align scout and localizer,
2) GE EPI with posterior-anterior (PA) phase encoding direction (3 TRs; Figure 1B),
3) first GE EPI with anterior-posterior (AP) phase encoding direction (324 TRs; Figure 1A),

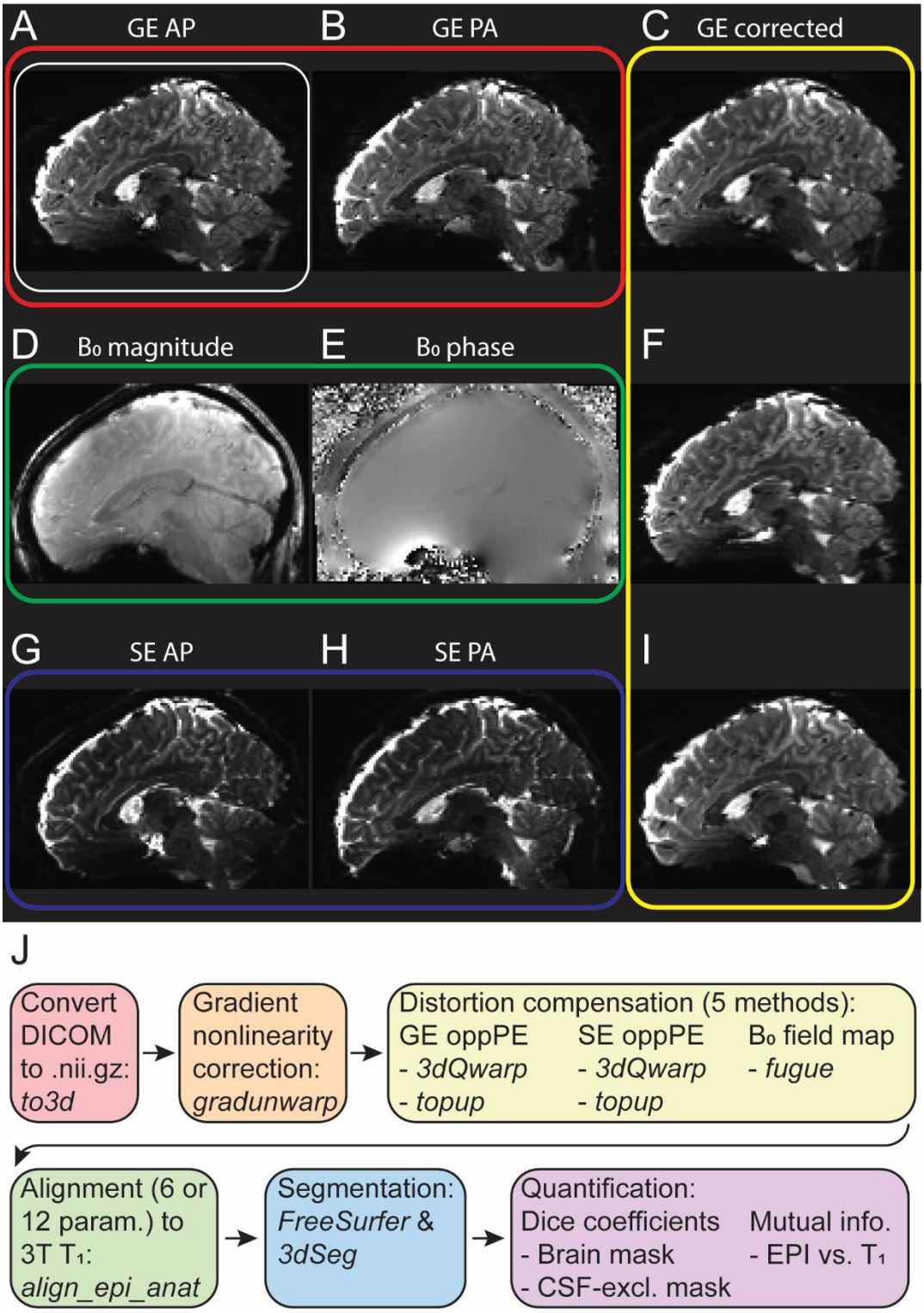

Figure 1. Data and processing pipeline. **A** & **B**) Gradient echo (GE) data with opposite (anterior-posterior [AP] and posterior-anterior [PA], respectively) phase encoding directions. White box in **A** indicates that the GE AP data were the base data set to which all distortion compensation methods were applied. All brain images are examples from the same parasagittal section in the same subject, after gradient nonlinearity correction has been applied. **C**) GE data after applying distortion compensation based on GE oppPE field map. **D** & **E**) B_0 field map magnitude and phase data, respectively. **F**) GE data after applying distortion compensation based on B_0 field map. **G** & **H**) Spin echo (SE) oppPE data (AP & PA, respectively). **I**) GE data after applying distortion compensation based on SE oppPE field map. **J**) Data processing pipeline steps and software (italics). Arrows indicate the sequence in which processing steps were performed.

Table 1. Scan parameters. Anat. = anatomical, TR = repetition time, TE = echo time, FOV = field of view, iso. = isotropic.

Scan	Field	TR	TE	Echo spacing	Flip angle	Resolution	Partial Fourier	Slices	FOV (mm)
GE EPI	7T	1000 ms	22.2 ms	0.64 ms	45°	1.6 mm iso.	7/8	85	208 x 208
B_0 field map	7T	642 ms	4.08 / 5.1 ms	-	32°	1.6 mm iso.	6/8	85	208 x 208
SE EPI	7T	3000 ms	60 ms	0.64 ms	90° / 180°	1.6 mm iso.	7/8	85	208 x 208
T_1 anat.	3T	2500 ms	1.81 / 3.6 / 5.39 / 7.18 ms	11.2 ms	8°	0.8 mm iso.	Off (phase) & 6/8 (slice)	208	256 x 256
T_2 anat.	3T	3200 ms	564 ms	3.86 ms	Variable	0.8 mm iso.	Allowed (phase) & off (slice)	208	256 x 256

4) second AP GE scan (297 TRs),
5) B_0 field mapping scan (Figure 1D & E),
6) AP SE scan (3 TRs; Figure 1G),
7) PA SE scan (3 TRs; Figure 1H),
8) third AP GE scan (468 TRs).

Inhomogeneity in the B_0 field was minimized prior to 7T fMRI data acquisition using the Siemens automated B_0 shimming procedure. Shim currents were calculated to minimize field variation within a 130 x 170 x 120 mm^3 region (i.e., the adjust volume) with an oblique-axial orientation centered on the brain (standardized by Auto Align). To assess shim quality, the linewidth of water (full width at half-maximum [FWHM]) was measured in the Siemens Interactive Shim tab during each scanning session before fMRI data were acquired (for this study, mean linewidth across subjects = 60 Hz, *SD* = 11 Hz). Shim values were stored and applied across all scanning runs using a 3rd-party stand-alone program (*shimcache*), to prevent any accidental loss of the B_0 shim between scans.

3T structural MRI data were acquired on a Siemens MAGNETOM Prisma scanner (software version: VE11C). This scanner was equipped with two RF power amplifiers with a combined power of 40 kW, and body gradients with 80 mT/m maximum amplitude and 200 T/m/s maximum slew rate. Data were acquired using a Siemens 32 channel radio frequency head coil. T_1- and T_2-weighted anatomical scans (parameters listed in Table 1) were acquired in the first of two 3T MRI scanning sessions.

Data analysis and statistics

Our data processing pipeline is summarized in Figure 1J. All data processing steps were performed using either AFNI[31] (version 18.2.04) or FSL[30] (version 5.0.9), as noted below. Data were converted from DICOM to g-zipped NIFTI format using AFNI's *to3d* program. To obtain a single time point for all EPI scans for the sake of computational efficiency, we took the temporal median of 3 TRs at the beginning or end of each scan (i.e., the time points closest to the respective field map scan(s), see below) using AFNI's *3dTstat*. We then performed gradient nonlinearity unwarping using *gradunwarp* (version 1.0.3; github.com/Washington-University/gradunwarp), with the warp field (a.k.a. voxel displacement map) applied using AFNI's *3dNwarpApply*. In our typical analysis path (i.e., in other studies), we apply all geometric corrections within a single resampling step to minimize blurring. In the current study, we first applied gradient nonlinearity correction and then separately applied B_0 inhomogeneity distortion compensation, which allowed us to specifically examine the performance of B_0 inhomogeneity distortion correction methods implemented in AFNI versus FSL.

Distortion compensation

We then performed corrections for geometric distortion due to B_0 inhomogeneity on our 7T GE EPI data using each of the following 5 methods:

1) GE opposite phase encoding (oppPE) field map correction[14-16] via AFNI's *3dQwarp* or
2) FSL's *topup*. Distortion correction in each of these two methods was applied to the median of TRs 1-3 from the first AP GE EPI scan.
3) B_0 field map correction[4, 12, 13] in FSL's *fugue*, applied to the median of TRs 295-297 from the second AP GE scan.
4) SE oppPE field map correction using AFNI's *3dQwarp*, or

5) FSL's *topup*, applied to the median of TRs 1-3 from the third AP GE scan.

The details of each distortion compensation method are provided below (see Code and data availability for a link to our published code for full details). Note that these methods are all designed to correct geometric distortions in the PE direction only (on the order of several millimeters); distortions in the readout and through-slice directions (generally less than 0.1 mm)[12] are not corrected by these methods and are not considered further in the present study.

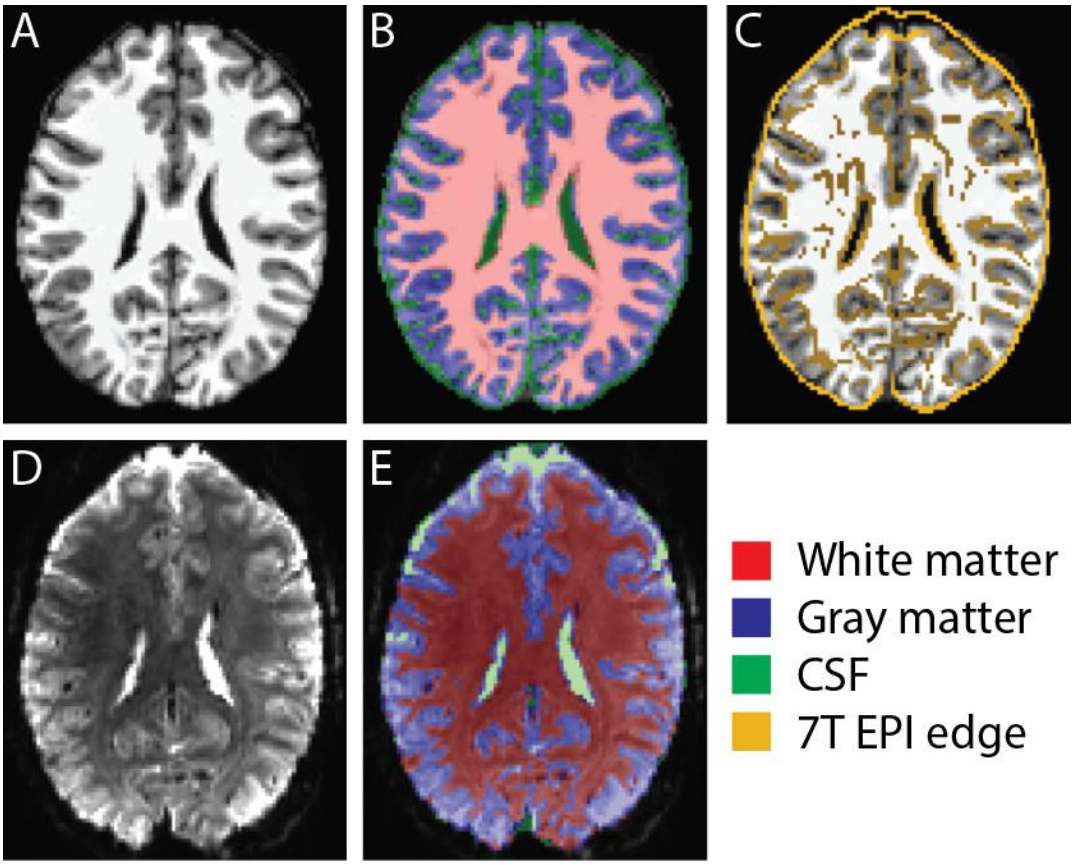

Figure 2. Alignment and segmentation of T_1 (**A**-**C**) and EPI data (**C**-**E**). Transparent colored overlays in **B** & **E** show binary masks for gray matter (blue), white matter (red), and cerebral spinal fluid (CSF; green) as a result of tissue segmentation. Yellow lines in **C** show edges from 7T GE EPI (using AFNI's *3dedge3*) overlaid on T_1 data, to show alignment. All brain images are examples from the same axial section in the same subject, after gradient nonlinearity correction, geometric distortion compensation, and co-registration.

For the GE and SE oppPE methods using AFNI's *3dQwarp*, both the AP and PA scans were masked using AFNI's *3dAutomask* to remove non-brain image regions. Next, the warp field for distortion compensation was calculated using *3dQwarp* with the *-plusminus* flag (indicating that the desired undistorted brain image is 'in between' the AP and PA scans). This program calculates distortion within image regions of progressively smaller size (minimum size used in our study was 9 mm), after progressive blurring using a spatial median filter (radius for our study was 0.08 to 1.6 mm, with less blur applied to smaller image regions). Distortion compensation of the GE EPI scan was then performed by applying the resulting warp field using AFNI's *3dNwarpApply* with sinc interpolation for the final resampling step.

For distortion based on GE and SE oppPE field maps using FSL's *topup*[14], the warp field was calculated using the default *topup* parameters (i.e., those provided by FSL within the *b02b0.cnf* file). This method also involves calculating geometric distortion across progressively smaller warp field regions (using B-splines; resolution was 19.2 to 3.2 mm in our study). Data were blurred across these progressive stages using a Gaussian kernel (FWHM ranged from 8 to 0 mm [i.e., no smoothing] for larger to smaller regions). Data for larger warp fields were sub-sampled by a factor of 2. Prior to *topup*, both the AP and PA scans were zero padded with 1 additional slice in the superior direction, to obtain an even number of slices (as required for voxel sub-sampling). Geometric distortion within the GE EPI scan was corrected based on the calculated warp field using FSL's *applytopup*, with cubic B-spline interpolation. The added empty slice was removed after distortion compensation.

For the B_0 field map method using FSL's *fugue*, non-brain regions of the magnitude portion of the B_0 field map were removed using FSL's *bet*. The difference between the phase portions of the B_0 field map scans with different echo times were exported by the scanner automatically. This phase difference map was then masked within the extracted brain region, converted from scanner units to radians per second using FSL's *fsl_prepare_fieldmap* tool (which also includes phase unwrapping), and then median filtered (radius = 1.6 mm) using AFNI's *3dMedianFilter* in order to reduce noise in

the field map, especially in regions near the outer edge of the brain. Distortion compensation of the GE EPI data was then performed using this phase map via FSL's *fugue*.

Our primary analysis (reported in the Analysis #1: main study section of the Results) assumes there was no head motion between each field map and the corresponding GE EPI scan, and that any difference between oppPE scan pairs is caused by geometric distortion and not head motion[4]. Prior to distortion compensation, no alignment between field map and GE EPI scans was performed, in order to avoid any spurious 'correction' of differences between scans that was in fact caused by geometric distortion. We performed an additional analysis, described below as Analysis #2, in order to examine the impact of this methodological decision.

Alignment

Following distortion compensation, we aligned GE EPI data and T_1 anatomical scans using AFNI's *align_epi_anat.py* function (Figure 2). Rigid body alignment (6-parameter: x, y, z, roll, pitch, yaw) was performed for the five distortion compensation methods above, as well as for non-distortion compensated (i.e., uncorrected) data. We used a rigid body alignment procedure in order to better preserve the geometric properties of the GE EPI and T_1 data sets, to facilitate clear comparison between the various distortion compensation methods. We also performed 12-parameter affine alignment (6 additional parameters for scaling and shearing) for the uncorrected data, in order to compare 6- versus 12-parameter alignment quality. We refer to the 12-parameter aligned data as 'alignment-only' since no explicit attempt was made to map and correct geometric distortion due to B_0 inhomogeneity in these data. However, we note that we were motivated to include the 12-parameter alignment method to determine the extent to which the addition of the 6 scaling and shearing parameters would mirror geometric distortion compensation performed with oppPE or B_0 field mapping methods. This procedure yielded a total of seven GE EPI data sets per subject for our analyses (five distortion compensated versions detailed above, plus 6- and 12-parameter alignment-only versions). We refer to these as the seven different analysis conditions below, as they form the basis of our comparison of different approaches for geometric distortion compensation.

Prior to alignment, the T_1 and T_2 anatomical data were processed using the HCP minimal pre-processing pipeline (version 3.22.0), including gradient nonlinearity correction with *gradunwarp* and skull stripping. Note that no correction for geometric distortion due to B_0 inhomogeneity was performed for these anatomical data, as any such distortions are expected to be minimal (< 0.1 mm)[21]. Although T_2-weighted scans have a more similar intensity profile to the GE EPI data, T_1 anatomical scans are currently more widely used in the field of human functional neuroimaging, and robust approaches for aligning EPI and T_1 data have been developed[43]. Thus, we chose to use the T_1-weighted scan as our anatomical reference in order to increase the generalizability of our results. We additionally corrected intensity inhomogeneities across the brain in the T_1 anatomical data using AFNI's *3dUnifize*.

Tissue segmentation

We performed tissue segmentation for each subject using the T_1 and T_2 anatomical scans to define individual white matter and pial surfaces in FreeSurfer[44, 45] (version 5.3.0) as part of the HCP minimal pre-processing pipeline (Figure 2A & B). For GE EPI data from each of the seven analysis conditions in each subject, we transformed both the T_1 and FreeSurfer's segmentation data (*wmparc*) into the space of the GE EPI scan using the alignment information (obtained above) via AFNI's *3dAllineate*. Individual binary masks for gray matter and white matter were defined from the T_1 data based on FreeSurfer's anatomical labels (surfer.nmr.mgh.harvard.edu/fswiki/FsTutorial/AnatomicalROI/FreeSurferColorLUT). To define binary masks for cerebral spinal fluid (CSF), we summed the gray and white matter masks from FreeSurfer, blurred the summed data using AFNI's *3dmerge* (FWHM = 0.5 mm), and then masked the blurred data at a value of 0.2 to create a binary mask that included the region surrounding the brain (putative CSF). We then summed this mask with a binary mask of the ventricles from FreeSurfer's *wmparc* file, and subtracted the gray and white matter masks to obtain a CSF mask. Gray matter, white matter, and CSF masks from the T_1 anatomy were used to aid segmentation of the 7T GE EPI data (below).

To segment the 7T fMRI data into gray matter, white matter, and CSF regions (Figure 2D & E), we first corrected spatial inhomogeneities in the GE EPI data using AFNI's *3dUnifize*, and then derived a whole-brain mask using AFNI's *3dAutomask*. We then segmented the 7T fMRI data from each analysis condition in each subject into gray matter, white matter, and CSF using AFNI's *3dSeg* function, with the gray matter, white matter, and CSF masks from the T_1 scan (above) as seed data.

Tissue masks from the 7T fMRI data were median filtered with a radius of 1.6 mm using AFNI's *3dMedianFilter* to reduce noise.

Dice coefficients

To quantify alignment between T_1 anatomical and GE EPI data (and thus the effectiveness of distortion compensation), we calculated the overlap between each subject's T_1 and fMRI data in each of the seven analysis conditions using Dice coefficients via AFNI's *3ddot* function. The Dice coefficient is a measure of how well two binary datasets overlap in three-dimensional space. This metric varies between zero (no overlap) and one (identity) and is calculated by taking the intersection of the two data sets, multiplying by two, and then dividing by the total number of voxels in both scans. Dice coefficients were calculated using two different types of binary masks of the 3T and 7T data: 1) a whole-brain mask using AFNI's *3dAutoMask*, and 2) a CSF-excluded mask based on the segmented T_1 and fMRI data.

Mutual information

We also quantified alignment quality by calculating mutual information between the T_1 and fMRI data for each of the seven analysis conditions in each subject. This metric, which comes from the information theory literature, reflects the similarity of two data sets by quantifying how much is learned about the second data set from knowing a value in the first. Mutual information is often used to assess multi-modal brain image registration[46], and should be maximal for two identical data sets that are perfectly aligned. Specifically, mutual information is defined as the difference between the joint entropy and the sum of the marginal entropies for two datasets. Compared to Dice coefficients, mutual information is more sensitive to differences in alignment in internal brain structures. Prior to calculating mutual information, we excluded non-brain regions of the T_1 and EPI data using the whole-brain masks described above (intensity values for regions outside the mask were set to zero). We computed mutual information using the *mutInfo* function (mathworks.com/matlabcentral/fileexchange/35625-information-theory-toolbox).

Additional analyses

We carried out a second analysis (Analysis #2: pre-aligned data) to explore whether differences in head motion across different field map scans may have affected our results. For example, if subjects moved more between and/or during scans that occurred later in the session, then this could have resulted in poorer distortion compensation using certain methods, given that our field map scans were acquired in a fixed order. To minimize differences between scans due to head motion, the following scans were aligned to the magnitude portion of the B_0 field map using AFNI's *align_epi_anat.py* function: 1) AP GE EPI, 2) PA GE EPI, 3) AP SE EPI, 2) PA SE EPI. Unlike our main analysis above, this procedure assumes that residual head motion between field map scans and fMRI data can be corrected by co-registration to a common reference scan, and that following such an alignment, differences between pairs of field map scans with opposite phase encoding directions reflect geometric distortion due to B_0 inhomogeneity. Distortion compensation was performed as described above, except that all distortion compensation methods were applied to a single GE EPI scan with AP PE direction (rather than applying distortion compensation to the GE EPI scan acquired closest in time to the corresponding field map scan, as in our main analysis).

In our third analysis (Analysis #3: single-band reference) we examined the role of image contrast in our results by using the single-band reference scan data that were acquired at the beginning of each multi-band 7T GE EPI scan. Image contrast (i.e., white matter vs. gray matter vs. CSF) was higher in the single-band reference as compared to the multi-band data (Supplemental Figure 1). This analysis was identical to the first, except that the single-band reference data were used in place of the multi-band 7T GE EPI data during alignment, EPI segmentation, and the quantification of alignment quality using Dice coefficients and mutual information (but were not used to calculate distortion fields). Using the single-band reference data for alignment purposes allowed us to examine the extent to which alignment quality (and thus, our Dice coefficient and mutual information metrics) depended on image contrast. This analysis of the single-band reference data also allowed us to assess whether our EPI segmentation method was limited by image contrast for the multi-band data in our main analysis.

All data were visualized in AFNI using default settings for display purposes (i.e., image histograms are scaled so that black ≤ 2%, white ≥ 98%). Brain images are shown in neurological convention (i.e., left is left).

Statistics

Statistical analyses were performed in MATLAB (version 2017b). Analyses of variance (ANOVAs) were performed using the *anovan* function, with subjects treated as a random effect, and the 7 analysis conditions (i.e., the 5 different distortion compensation methods, plus the 6- and 12-parameter alignment-only data) as a within-subjects factor. Normality and homogeneity of variance were assessed by visual inspection of the data (Supplemental Figure 2). Post-hoc comparisons between analysis methods were performed using paired 2-tailed *t*-tests, with False Discovery Rate (FDR) correction for 21 multiple comparisons (between each of the 7 analysis conditions). Because the effects of interest (i.e., differences between distortion compensation methods) were within- rather than between-subjects, we used within-subjects error bars to visualize the variance in each analysis condition, thereby excluding the between-subjects variance for display purposes. To do so, we used an established method[1] that involved subtracting the mean value for each subject (across all analysis conditions) from all data points for that individual, and then adding the grand mean (across all subjects and conditions).

Code and data availability

Our analysis code is available on GitHub (github.com/mpschallmo/DistortionCompensation). Imaging data are available from the Human Connectome Project (intradb.humanconnectome.org; first data release planned for 4th quarter, 2020).

Results

Analysis #1: main study

To compare different distortion compensation methods, we first examined the overlap between whole-brain masks obtained from 7T GE EPI data that had been corrected for geometric distortion and T_1-weighted anatomical data (T_1 hereafter), following co-registration. Data from 7 different analysis conditions were examined (Figure 1J), including those obtained using five different distortion correction methods, and two alignment-only data sets (6- and 12-parameter alignment). Overlap was calculated using the Dice coefficient, such that higher Dice coefficients reflect more-effective distortion compensation.

Dice coefficients for the whole-brain masks differed significantly across analysis conditions ($F_{6,30} = 42.7$, $p = 4 \times 10^{-32}$), as shown in Figure 3A (see also Supplemental Figure 2 for a visualization of all data points). This indicates that the method of distortion compensation significantly affected the degree to which whole-brain masks from EPI and T_1 anatomical scans overlapped. Post-hoc paired *t*-tests (FDR corrected for 21 comparisons between conditions) revealed that the overlap between EPI and T_1 anatomical masks was highest and comparable for the two GE oppPE methods using AFNI's *3dQwarp* and FSL's *topup* (red symbols). Dice coefficients were lower when using the B_0 field map (using FSL's *fugue*; green triangle) and SE oppPE (via *3dQwarp*; blue square). Note that in Figure 3, gray lines indicate conditions that do *not* differ significantly based on post-hoc tests (i.e., conditions that *do* differ significantly are *not* linked by gray lines; all significant paired t_{30} values ≥ 2.82, FDR-corrected *p*-values ≤ 0.042). Lower Dice coefficients were observed for the SE oppPE data corrected using *topup* (blue triangle), which did not differ from the uncorrected data using only a 6-parameter alignment (white circle). Dice coefficients for whole-brain masks were lowest for the data using a 12-parameter alignment only (gray circle).

Next, we asked which distortion compensation method(s) performed best in terms of aligning binary tissue masks from fMRI and T_1 data with CSF regions excluded, rather than whole-brain masks (see Methods). This analysis was somewhat more sensitive to the alignment of internal brain structures, as compared to our previous analysis based on Dice coefficients for whole-brain masks. Dice coefficients for CSF-excluded masks varied significantly across different analysis conditions ($F_{6,30} = 91.5$, $p = 5 \times 10^{-52}$; Figure 3B), showing that the agreement between non-CSF brain regions from the EPI and T_1 anatomical scans depended on the method of distortion compensation that was used. Post-hoc paired *t*-tests revealed that the overlap for non-CSF regions was highest when using GE oppPE field maps for distortion compensation (via either AFNI's *3dQwarp* or FSL's *topup*; red symbols; all significant paired t_{30} values ≥ 2.84, FDR-corrected *p*-values ≤ 0.032). The overlap for the CSF-excluded masks was lower when distortion compensation was performed using a B_0 field map (via FSL's *fugue*; green triangle) or SE oppPE field map (in either AFNI's *3dQwarp* or FSL's *topup*; blue symbols), and lowest for the alignment-only data (using either 6-parameter [white circle] or 12-parameter alignment methods [gray circle]).

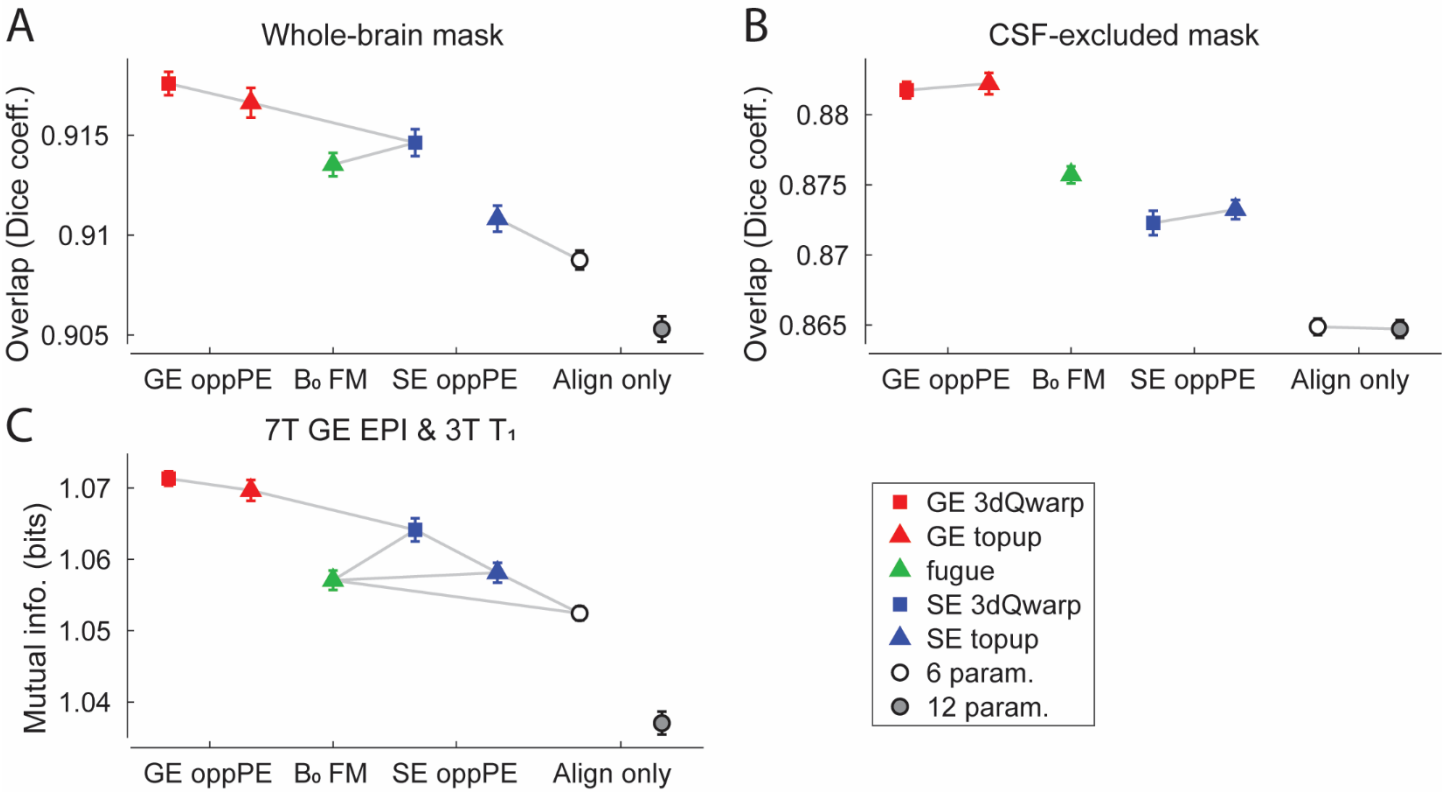

Figure 3. Main results. **A**) Overlap (Dice coefficient) between GE EPI and T_1 brain mask data, across different distortion compensation methods. Gray lines indicate conditions that do *not* differ significantly (post-hoc paired *t*-tests, threshold $p < 0.05$, FDR corrected). X-axis labels: GE oppPE = gradient echo opposite phase encoding field map (red), B_0 FM = B_0 field map (green), SE oppPE = spin echo opposite phase encoding field map (blue), Align only = alignment-only (no explicit geometric distortion compensation). **B**) Same, but for binary masks with regions of cerebrospinal fluid (CSF) excluded, following tissue segmentation. **C**) Mutual information between GE EPI and T_1 scan data. Squares show data corrected using AFNI, triangles show data from FSL, circles show alignment-only data. Error bars are *SEM* calculated within subjects[1]. All of the tested distortion compensation methods improved agreement between fMRI and T_1 data sets. For our particular dataset, GE oppPE field maps (red) tended to produce the best results.

We further compared distortion compensation methods by calculating the mutual information between fMRI and T_1 data, as higher mutual information reflects better alignment. Compared to the Dice coefficient, mutual information is more sensitive to differences in the alignment of internal brain structures, as it is based on the intensity of all voxels within the brain. Mutual information between EPI and T_1 anatomical scans differed significantly across analysis conditions ($F_{6,30} = 35.1$, $p = 7 \times 10^{-28}$; Figure 3C), reflecting a difference in alignment quality for different distortion compensation methods. In particular, post-hoc tests revealed that mutual information was highest when using the GE oppPE field map methods for distortion compensation (red squares; all significant paired t_{30} values ≥ 3.48, FDR-corrected *p*-values ≤ 0.017). Mutual information was generally comparable between all other methods and the 6-parameter alignment-only data (white square). The 12-parameter alignment-only method (gray circle) yielded lower mutual information compared to all other conditions.

Analysis #2: pre-aligned data

Human subjects, especially those who are not experienced with MR scanning, may be more likely to move, or move more towards the end of a long scanning session. Because our scans were acquired in a fixed order, we considered whether differences in head motion might have biased our results in favor of the GE oppPE data, which was acquired near the beginning of the session (approximately 1.25 hours in total length), rather than the B_0 field map or SE oppPE data, which were acquired near the end. Specifically, if subjects tended to move more during the B_0 field map and SE oppPE scans, or moved more between these scans and the GE EPI scans on which distortion compensation was performed, then this might degrade the quality of distortion compensation for the B_0 field map and SE oppPE methods as compared to the GE oppPE method.

To explore this issue, we re-ran our analyses after aligning all field map and 7T GE fMRI scans to the magnitude portion of the B_0 field map (see Methods for details, and a discussion of why this initial alignment step was omitted from the first analysis). We applied all five distortion compensation methods to the same 7T GE EPI scan, to mitigate any possible bias caused by the fixed scanning order. We found that this methodological decision had very little impact on our results (Supplemental Figure 3); all distortion compensation methods improved alignment between fMRI and T_1 data (ANOVAs, main effects of condition for whole-brain masks, CSF-excluded masks, and mutual information, $F_{6,30} > 35.7$, p-values $< 3 \times 10^{-28}$), with the GE oppPE field maps showing the strongest performance.

Analysis #3: single-band reference

Alignment and segmentation of GE EPI data may depend on image contrast (e.g., gray matter vs. white matter intensity). To explore the role of image contrast in our results, we repeated our main analyses using the single-band reference data in place of the multi-band 7T GE EPI data for alignment, segmentation, and quantification purposes, as image contrast was higher in the single-band reference (Supplemental Figure 1). We calculated Dice coefficients and mutual information between the GE single-band reference data and the T_1 scans, as before. These metrics differed significantly across distortion compensation methods for the single-band reference data (ANOVAs, main effects of condition, $F_{6,30} > 35.2$, p-values $< 5 \times 10^{-28}$; Supplemental Figure 4). The patterns of results for the single-band reference data were very similar to those obtained with multi-band GE EPI in the main analysis (Figure 3), suggesting that the quality of the alignment and segmentation of our 7T data were not limited by image contrast in the multi-band scans.

Discussion

Our analyses showed that all of the distortion compensation methods tested (GE oppPE field maps, B_0 field maps, SE oppPE field maps) yielded improved correspondence between GE fMRI and T_1 anatomical data, compared to alignment-only data. We found no substantial differences when comparing our results for oppPE field map corrections performed using AFNI versus FSL (squares vs. triangles, Figure 3), suggesting that these two software packages yield equivalent data quality for this type of distortion compensation. However, we did find small but consistent differences in Dice coefficients and mutual information between the various distortion compensation methods we examined. Agreement between GE fMRI and T_1 data was generally highest in our data set when using GE oppPE field maps for distortion compensation (red symbols, Figure 3). Hence, we have chosen to implement this particular correction method within our own internal data processing pipeline for the Psychosis Human Connectome Project.

This study provides a framework for deciding which distortion compensation method to use for a given data set, based on quantitative comparisons of the agreement between distortion-corrected EPI data and a T_1 anatomical reference scan. We expect that the relative performance of different methods may vary across data sets based on data acquisition parameters, scanner and coil hardware, and the details of the processing pipeline that is used. Thus, the reader may wish to compare the relative performance of different distortion compensation methods in their own dataset, using an approach similar to ours. We used multiple metrics to quantify EPI-T_1 agreement as a proxy for correction quality (i.e., Dice coefficients for whole-brain masks and CSF-excluded masks, as well as mutual information), since we acknowledge that there is no single gold standard for measuring the quality of distortion compensation in human brain imaging data[28] (but see the following studies that used simulations to try to establish ground truth[47, 48]). By making our data and analysis code publicly available (see Methods), we hope to facilitate the empirical selection of effective approaches for geometric distortion compensation in future research.

In addition to geometric distortion compensation, our analyses included gradient nonlinearity correction[2, 3, 41], a post-processing step to correct for static spatial non-uniformities in the brain images caused by the gradients themselves (i.e., not dependent on the scanning sequence or B_0 field inhomogeneity). This is particularly important in cases such as ours, where one wishes to align EPI data acquired on one scanner to anatomical data acquired on another, as gradient nonlinearities will vary across scanners based on differences in gradient hardware. Previous studies comparing different geometric distortion compensation methods have generally not included (or reported) gradient nonlinearity correction. For datasets acquired using a single scanner, sequence-independent gradient nonlinearities limit geometric fidelity but not the ability to align distortion corrected EPI to anatomical reference scans. We believe that effective corrections for both gradient nonlinearities and geometric distortions are critical for achieving high spatial fidelity, and for harmonizing EPI and T_1 data across different scanners and field strengths.

It has been suggested that, due to reduced through-slice dephasing, SE oppPE field maps may provide higher quality distortion compensation as compared to GE oppPE field maps[34]. However, in the current study we observed consistently better distortion correction, as quantified by Dice coefficients and mutual information, for GE vs. SE oppPE methods when applied to our GE EPI data (red vs. blue symbols, Figure 3). We offer two possible explanations, which are not mutually exclusive. First, there may be more opportunities for head motion to degrade the quality of distortion compensation when using a SE oppPE field map to correct GE EPI data, as there are two additional scans (beyond the GE EPI to be corrected) during and between which the subject must hold still, versus only one additional scan for a GE oppPE field map (i.e., the GE EPI data used for functional imaging themselves can serve as half of the GE oppPE pair). As noted below, any head motion between scans will change the B_0 inhomogeneities and subsequent geometric distortions, leading to poorer correction. Second, superior performance of the GE oppPE field maps might possibly be due to differences in signal intensity between GE and SE data (compare Figure 1A & B vs. Figure 1G & H). Unwarping algorithms (i.e., FSL's *topup* and AFNI's *3dQwarp*) may be generally better suited to correcting geometric distortion based on the image contrast in GE vs. SE data. Additionally, in regions of significant B_0 inhomogeneity (e.g., temporal lobe, orbitofrontal cortex), geometric distortion may cause displaced signal from multiple voxels to 'pile up' within a single voxel[14, 18, 19, 27]. If the signal intensity differs strongly between the pair of oppPE scans from which the voxel displacement map is calculated and the EPI scan to which it is applied (e.g., when using SE oppPE field maps to correct distortion in GE EPI), then the voxel displacement map in such regions might be incorrect, resulting in poorer distortion compensation[15, 48].

Our results agree with previous studies that have universally shown corrections for geometric distortion due to B_0 field inhomogeneity improve EPI data quality and alignment with minimally distorted reference scans[4]. In particular, previous work has generally shown better performance for oppPE field map strategies, as compared to B_0 field maps, which has been attributed in part to the difficulty of using B_0 field maps to correct distortion near the edges of the brain (see Figure 1F), where phase values change rapidly. Using simulated EPI data, both Esteban[47] and Graham[48] showed quantitatively that ground truth undistorted images were recovered best using an oppPE field map method, whereas B_0 field maps performed slightly worse, and nonlinear registration-based methods were greatly inferior (but still better than no correction at all). Similar conclusions were reached by Hong and colleagues[28] using SE EPI in the mouse brain at 7T, by Holland and colleagues[34] using SE EPI at 1.5 and 3T in the human brain, and by Wang and colleagues[49] using 3T dMRI data in humans (see also [5]). Thus, there is some evidence to suggest, in general terms, better performance for oppPE methods over B_0 field maps, with nonlinear registration yielding poorer results (but better than no correction, and useful in cases where the additional scans required to perform the other methods above are not available).

This study considered only static geometric distortions in the GE EPI data caused by B_0 inhomogeneity. If a subject moves during a scanning session, then the B_0 inhomogeneities will not be stable over time, and geometric distortions will vary with head motion[4], resulting in poorer correction based on static methods[48]. We conducted a second analysis (Analysis #2: pre-aligned data) in which all field map scans were first aligned to the magnitude portion of the B_0 field map prior to distortion compensation. The results from this second analysis (Supplemental Figure 3) recapitulated the findings from the main portion of our study (Figure 3), suggesting that differences in subject head motion over time may not explain the pattern of results we observed. Methods for dynamic distortion compensation (e.g., with different distortion fields calculated for each time point in an EPI time series) have also been proposed[6, 26, 29], and may offer advantages in correcting time-varying geometric distortion, as compared to the static approaches considered here. However, to our knowledge, such dynamic distortion compensation methods are not currently implemented in the software packages that are most often used to pre-process brain imaging data.

Acknowledgments

We thank Jesslyn (Li Shen) Chong, Tori Espensen-Sturges, Andrea N. Grant, Rohit S. Kamath, Timothy J. Lano, and Marisa J. Sanchez for their assistance with data collection. We also thank Phillip C. Burton, Bryon A. Mueller, and Hannah R. Moser for help with data processing, and Essa Yacoub for supporting the design of the study.

This work was supported by funding from the National Institutes of Health (U01 MH108150). Salary support for MPS was provided by K01 MH120278. Support for MR scanning at the University of Minnesota Center for Magnetic Resonance Research was provided by P41 EB015894 and P30 NS076408. This work used tools from the University of Minnesota Clinical and Translational Science Institute that were supported by UL1 TR002494.

Supplemental information

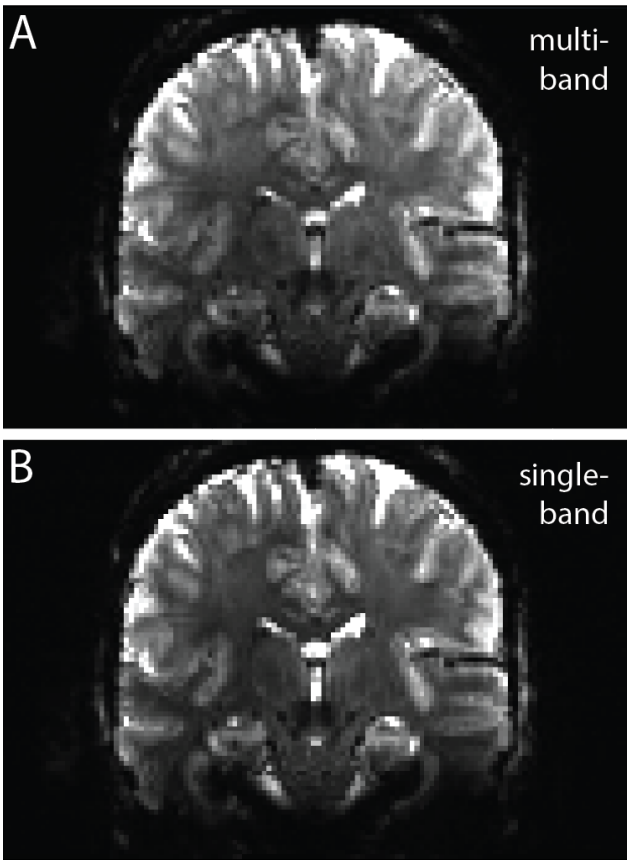

Supplemental Figure 1. Single-band reference data. Panel **A** shows an example re-sliced coronal section from our standard multi-band GE EPI sequence, whereas **B** shows the single-band reference data from the same section in the same subject. Note the higher gray matter-white matter contrast for the single-band reference data in **B**.

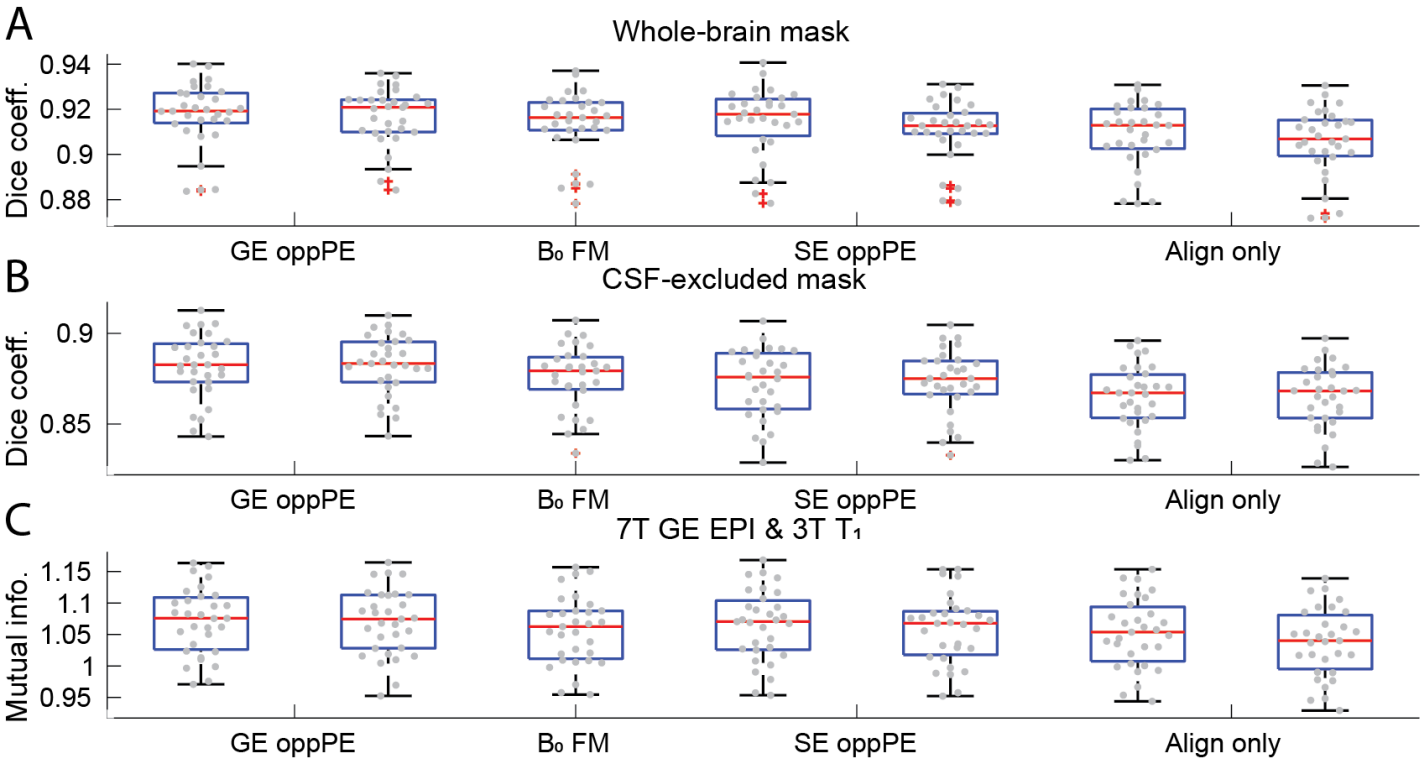

Supplemental Figure 2. Box plots of the results from the main analysis. The order of conditions (left to right) is GE 3dQwarp, GE topup, fugue, SE 3dQwarp, SE topup, 6 param., 12 param. (same as in Figure 3). X-axis labels: GE oppPE = gradient echo opposite phase encoding field map, B_0 FM = B_0 field map, SE oppPE = spin echo opposite phase encoding field map, Align only = alignment-only (no explicit geometric distortion compensation). Red lines = median, blue boxes = interquartile range, whiskers = 1.5 x interquartile range, red pluses = points outside whiskers, gray dots = all data points.

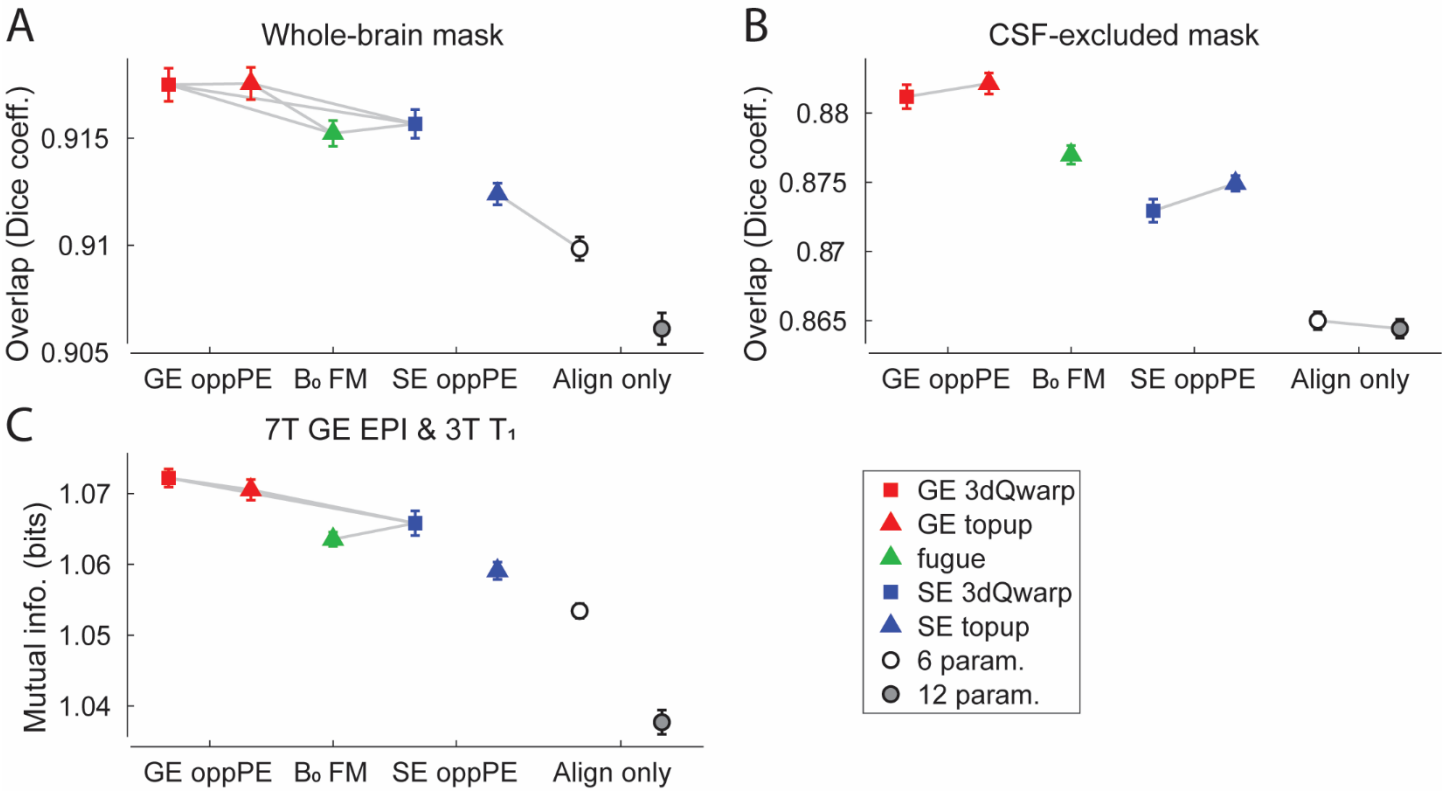

Supplemental Figure 3. Results for data aligned to B_0 field map from Analysis #2. **A**) Overlap (Dice coefficient) between GE EPI and T_1 brain mask data, across different distortion compensation methods. Gray lines indicate conditions that do *not* differ significantly (post-hoc paired *t*-tests, threshold $p < 0.05$, FDR corrected). X-axis labels: GE oppPE = gradient echo opposite phase encoding field map (red), B_0 FM = B_0 field map (green), SE oppPE = spin echo opposite phase encoding field map (blue), Align only = alignment-only (no explicit geometric distortion compensation). **B**) Same, but for binary masks with regions of cerebrospinal fluid (CSF) excluded, following tissue segmentation. **C**) Mutual information between GE EPI and T_1 scan data. Squares show data corrected using AFNI, triangles show data from FSL, circles show alignment-only data. Error bars are *SEM* calculated within subjects[1]. Aligning all scans to the magnitude portion of the B_0 field map did not substantially alter our pattern of results (compare with data from the main analysis in Figure 3), suggesting that differences in head motion across the scanning session did not dramatically affect our findings.

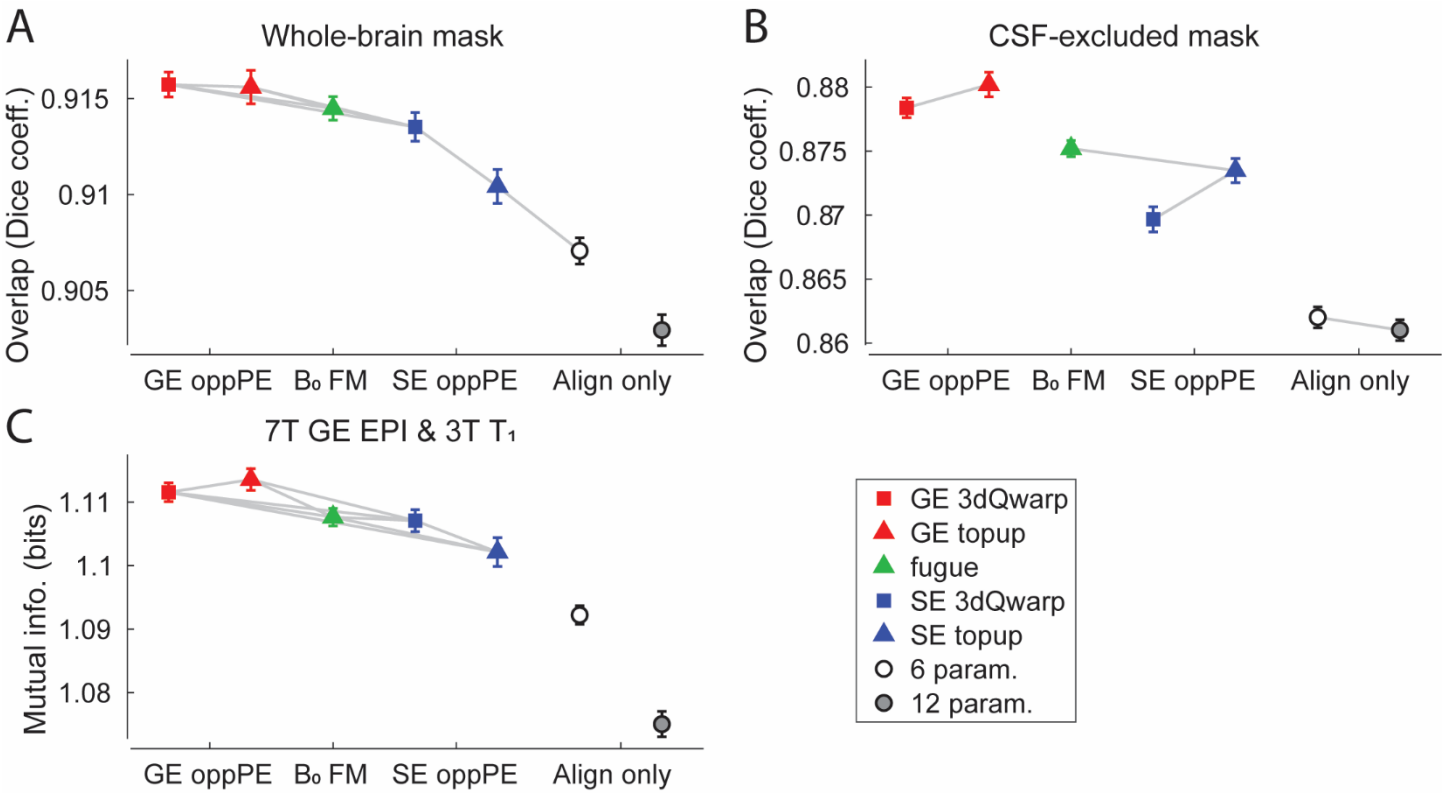

Supplemental Figure 4. Results for single-band reference data from Analysis #3. **A**) Overlap (Dice coefficient) between GE EPI and T_1 brain mask data, across different distortion compensation methods. Gray lines indicate conditions that do *not* differ significantly (post-hoc paired *t*-tests, threshold $p < 0.05$, FDR corrected). X-axis labels: GE oppPE = gradient echo opposite phase encoding field map (red), B_0 FM = B_0 field map (green), SE oppPE = spin echo opposite phase encoding field map (blue), Align only = alignment-only (no explicit geometric distortion compensation). **B**) Same, but for binary masks with regions of cerebrospinal fluid (CSF) excluded, following tissue segmentation. **C**) Mutual information between GE EPI and T_1 scan data. Squares show data corrected using AFNI, triangles show data from FSL, circles show alignment-only data. Error bars are *SEM* calculated within subjects[1]. Using the single-band reference data for alignment and segmentation did not dramatically alter the pattern of results (compare with data from the main analysis in Figure 3), suggesting that these analysis steps did not depend strongly on image contrast.

References

1. Morey, R.D. Confidence intervals from normalized data: A correction to Cousineau (2005). *Tutorial in Quantitative Methods for Psychology* **4**, 61-64 (2008).
2. Bakker, C.J.G., Moerland, M.A., Bhawandien, R. & Beersma, R. Analysis of machine-dependent and object-induced geometric distortion in 2DFT MR imaging. *Magnetic Resonance Imaging* **10**, 597-608 (1992).
3. Jezzard, P. & Clare, S. Sources of distortion in functional MRI data. 6 (1999).
4. Hutton, C.*, et al.* Image distortion correction in fMRI: A quantitative evaluation. *NeuroImage* **16**, 217-240 (2002).
5. Gholipour, A., Kehtarnavaz, N., Scherrer, B. & Warfield, S.K. On the accuracy of unwarping techniques for the correction of susceptibility-induced geometric distortion in magnetic resonance Echo-planar images. in *2011 33rd Annual International Conference of the IEEE Engineering in Medicine and Biology Society* 6997-7000 (IEEE, 2011).
6. Dymerska, B., Poser, B.A., Barth, M., Trattnig, S. & Robinson, S.D. A method for the dynamic correction of B 0 - related distortions in single-echo EPI at 7 T. *NeuroImage* **168**, 321-331 (2018).
7. McKinnon, G.C. Ultrafast interleaved gradient-echo-planar imaging on a standard scanner. *Magnetic Resonance in Medicine* **30**, 609-616 (1993).
8. Feinberg, D.A. & Oshio, K. Phase errors in multi-shot echo planar imaging. *Magnetic Resonance in Medicine* **32**, 535-539 (1994).
9. Moeller, S., Van de Moortele, P.-F., Goerke, U., Adriany, G. & U??urbil, K. Application of parallel imaging to fMRI at 7 Tesla utilizing a high 1D reduction factor. *Magnetic Resonance in Medicine* **56**, 118-129 (2006).
10. Olman, C.A., Davachi, L. & Inati, S. Distortion and dignal loss in medial temporal lobe. *PLoS ONE* **4**, e8160 (2009).
11. Glover, G.H. & Law, C.S. Spiral-in/out BOLD fMRI for increased SNR and reduced susceptibility artifacts. *Magnetic Resonance in Medicine* **46**, 515-522 (2001).
12. Jezzard, P. & Balaban, R.S. Correction for geometric distortion in echo planar images from B0 field variations. *Magnetic Resonance in Medicine* **34**, 65-73 (1995).
13. Hunsche, S.*, et al.* Optimized distortion correction of epi-based statistical parametrical maps for stereotactic neurosurgery. *Magnetic Resonance Imaging* **22**, 163-170 (2004).
14. Andersson, J.L.R., Skare, S. & Ashburner, J. How to correct susceptibility distortions in spin-echo echo-planar images: application to diffusion tensor imaging. *NeuroImage* **20**, 870-888 (2003).
15. Embleton, K.V., Haroon, H.A., Morris, D.M., Ralph, M.A.L. & Parker, G.J.M. Distortion correction for diffusion-weighted MRI tractography and fMRI in the temporal lobes. *Human Brain Mapping* **31**, 1570-1587 (2010).
16. Morgan, P.S., Bowtell, R.W., McIntyre, D.J.O. & Worthington, B.S. Correction of spatial distortion in EPI due to inhomogeneous static magnetic fields using the reversed gradient method. *Journal of Magnetic Resonance Imaging* **19**, 499-507 (2004).
17. Gholipour, A.*, et al.* Distortion correction via non-rigid registration of functional to anatomical magnetic resonance brain images. in *2006 International Conference on Image Processing* 1181-1184 (IEEE, 2006).
18. Li, Y.*, et al.* Physics-based constraints for correction of geometric distortions in gradient echo EP images via nonrigid registration. in *Medical Imaging* (ed. J.M. Reinhardt & J.P.W. Pluim) 61442I (2006).
19. Li, Y.*, et al.* Accounting for signal loss due to dephasing in the correction of distortions in gradient-echo EPI via nonrigid registration. *IEEE Transactions on Medical Imaging* **26**, 1698-1707 (2007).
20. Li, Y., Xu, N., Fitzpatrick, J.M. & Dawant, B.M. Geometric distortion correction for echo planar images using nonrigid registration with spatially varying scale. *Magnetic Resonance Imaging* **26**, 1388-1397 (2008).
21. Studholme, C., Constable, R.T. & Duncan, J.S. Accurate alignment of functional EPI data to anatomical MRI using a physics-based distortion model. *IEEE Transactions on Medical Imaging* **19**, 1115-1127 (2000).
22. Robson, M.D., Gore, J.C. & Constable, R.T. Measurement of the point spread function in MRI using constant time imaging. *Magnetic Resonance in Medicine* **38**, 733-740 (1997).
23. Zaitsev, M., Hennig, J. & Speck, O. Point spread function mapping with parallel imaging techniques and high acceleration factors: Fast, robust, and flexible method for echo-planar imaging distortion correction. *Magnetic Resonance in Medicine* **52**, 1156-1166 (2004).
24. Zeng, H. & Constable, R.T. Image distortion correction in EPI: Comparison of field mapping with point spread function mapping. *Magnetic Resonance in Medicine* **48**, 137-146 (2002).
25. Munger, P., Crelier, G.R., Peters, T.M. & Pike, G.B. An inverse problem approach to the correction of distortion in EPI images. *IEEE Transactions on Medical Imaging* **19**, 681-689 (2000).

26. Andersson, J.L.R., Hutton, C., Ashburner, J., Turner, R. & Friston, K. Modeling geometric deformations in EPI time series. *NeuroImage* **13**, 903-919 (2001).
27. Wan, X., Gullberg, G.T., Parker, D.L. & Zeng, G.L. Reduction of geometric and intensity distortions in echo-planar imaging using a multireference scan. *Magnetic Resonance in Medicine* **37**, 932-942 (1997).
28. Hong, X., To, X.V., Teh, I., Soh, J.R. & Chuang, K.-H. Evaluation of EPI distortion correction methods for quantitative MRI of the brain at high magnetic field. *Magnetic Resonance Imaging* **33**, 1098-1105 (2015).
29. Barry, R.L.*, et al.* Evaluation of preprocessing steps to compensate for magnetic field distortions due to body movements in BOLD fMRI. *Magnetic Resonance Imaging* **28**, 235-244 (2010).
30. Smith, S.M.*, et al.* Advances in functional and structural MR image analysis and implementation as FSL. *NeuroImage* **23**, 208-219 (2004).
31. Cox, R.W. AFNI: software for analysis and visualization of functional magnetic resonance neuroimages. *Computers and Biomedical Research* **29**, 162-173 (1996).
32. Friston, K.J.*, et al.* Statistical parametric maps in functional imaging: A general linear approach. *Human Brain Mapping* **2**, 189-210 (1994).
33. Goebel, R., Esposito, F. & Formisano, E. Analysis of functional image analysis contest (FIAC) data with brainvoyager QX: From single-subject to cortically aligned group general linear model analysis and self-organizing group independent component analysis. *Human Brain Mapping* **27**, 392-401 (2006).
34. Holland, D., Kuperman, J.M. & Dale, A.M. Efficient correction of inhomogeneous static magnetic field-induced distortion in Echo Planar Imaging. *NeuroImage* **50**, 175-183 (2010).
35. Olman, C.A. & Yacoub, E. High-field fMRI for human applications: An overview of spatial resolution and signal specificity. *The Open Neuroimaging Journal* **5**, 74-89 (2011).
36. Van Essen, D.C.*, et al.* The WU-Minn Human Connectome Project: An overview. *NeuroImage* **80**, 62-79 (2013).
37. Vu, A.T.*, et al.* High resolution whole brain diffusion imaging at 7 T for the Human Connectome Project. *NeuroImage* **122**, 318-331 (2015).
38. Glasser, M.F.*, et al.* The Human Connectome Project's neuroimaging approach. *Nature Neuroscience* **19**, 1175-1187 (2016).
39. T. Vu, A.*, et al.* Tradeoffs in pushing the spatial resolution of fMRI for the 7T Human Connectome Project. *NeuroImage* **154**, 23-32 (2017).
40. Benson, N.C.*, et al.* The Human Connectome Project 7 Tesla retinotopy dataset: Description and population receptive field analysis. *Journal of Vision* **18**, 23 (2018).
41. Glasser, M.F.*, et al.* The minimal preprocessing pipelines for the Human Connectome Project. *NeuroImage* **80**, 105-124 (2013).
42. Jeste, D.V.*, et al.* A new brief instrument for assessing decisional capacity for clinical research. *Archives of general psychiatry* **64**, 966-974 (2007).
43. Saad, Z.S.*, et al.* A new method for improving functional-to-structural MRI alignment using localPearson correlation. *NeuroImage* **44**, 839-848 (2009).
44. Dale, A.M., Fischl, B. & Sereno, M.I. Cortical surface-based analysis. I. Segmentation and surface reconstruction. *NeuroImage* **9**, 179-194 (1999).
45. Dale, A.M. & Sereno, M.I. Improved localization of cortical activity by combining EEG and MEG with MRI cortical surface reconstruction: A linear approach. *Journal of Cognitive Neuroscience* **5**, 162-176 (1993).
46. Studholme, C., Hill, D.L.G. & Hawkes, D.J. An overlap invariant entropy measure of 3D medical image alignment. *Pattern Recognition* **32**, 71-86 (1999).
47. Esteban, O.*, et al.* Simulation-based evaluation of susceptibility distortion correction methods in diffusion MRI for connectivity analysis. in *2014 IEEE 11th International Symposium on Biomedical Imaging (ISBI 2014)* 738-741 (IEEE, 2014).
48. Graham, M.S., Drobnjak, I., Jenkinson, M. & Zhang, H. Quantitative assessment of the susceptibility artefact and its interaction with motion in diffusion MRI. *PLOS ONE* **12**, e0185647 (2017).
49. Wang, S.*, et al.* Evaluation of field map and nonlinear registration methods for correction of susceptibility artifacts in diffusion MRI. *Frontiers in Neuroinformatics* **11** (2017).